

Article

# Spatio-Temporal Variation of Total Nitrogen and Ammonia Nitrogen in the Water Source of the Middle Route of the South-To-North Water Diversion Project

Guoquan Dong <sup>1</sup>, Zhenqi Hu <sup>1,2,\*</sup>, Xuan Liu <sup>3</sup> , Yaokun Fu <sup>1</sup> and Wenjing Zhang <sup>4</sup>

<sup>1</sup> School of Geosciences and Surveying Engineering, China University of Mining and Technology (Beijing), Beijing 100083, China; bqt1700204048@student.cumtb.edu.cn (G.D.); falcone@163.com (Y.F.)

<sup>2</sup> School of Environment Science and Spatial Information, China University of Mining and Technology, Xuzhou 221116, China

<sup>3</sup> School of Surveying and Land Information Engineering, Henan Polytechnic University, Jiaozuo 454000, China; keystone1x@hpu.edu.cn

<sup>4</sup> Department of Surveying and Mapping Engineering, Henan college of surveying and mapping, Zhengzhou 454000, China; zhangwenjing@hpu.edu.cn

\* Correspondence: huzq@cumtb.edu.cn

Received: 7 August 2020; Accepted: 16 September 2020; Published: 18 September 2020



**Abstract:** The quantitative inversion of the concentrations of water quality parameters could clarify the temporal and spatial distribution characteristic, migration, and conversion of water quality parameters. This study took the Danjiangkou Reservoir as the research object, and established an inversion model based on the reflectance of different band combinations of remote sensing analyses on Sentinel-2 images, combined with the water quality monitoring data of total nitrogen (TN) and ammonia nitrogen (NH<sub>3</sub>-N) of the sampling sites in February 2016. The inversion results of TN and NH<sub>3</sub>-N in 2020 were obtained, the variation of TN and NH<sub>3</sub>-N concentrations in the reservoir area were analyzed, and the factors accounting for the variation were discussed. The results indicated that the fitting accuracy using the established model was high for both TN and NH<sub>3</sub>-N, and R<sup>2</sup> was 0.782 for TN and 0.851 for NH<sub>3</sub>-N, respectively, showing high predication accuracy, which could be suitable for remote sensing inversion of TN and NH<sub>3</sub>-N concentrations in the Danjiangkou Reservoir. The NH<sub>3</sub>-N concentration of the Danjiangkou Reservoir was in line with Class I from 2016 to 2020, while the TN concentration was between Class III and IV. The inter-annual changes indicated that the overall water quality had an upward trend. The main tributary in the northern of the Danjiangkou Reservoir had a heavy load of TN, and after entering the reservoir, the flow velocity decreased, which caused nitrogen to accumulate at the river entrance, leading to a high TN concentration. The large slope of the mountainous area cause soil erosion. The lost soil and water carried a large amount of pesticides and fertilizers, and the ground runoff carried a large amount of nitrogen into water body, which could account for the high NH<sub>3</sub>-N concentration on the east and west sides of the southern part of the Danjiangkou Reservoir.

**Keywords:** remote sensing inversion; Sentinel-2 remote sensing image; total nitrogen; ammonia nitrogen; water source of the South-to-North Water Diversion Project (SNWDP)

## 1. Introduction

The South-to-North Water Diversion Project (SNWDP) is a major strategic infrastructure aimed at optimizing allocation of water resources across the river basin and benefiting the greatest number of people in China, and is the inter-basin water diversion project with major international influence [1]. The Danjiangkou Reservoir, as the water source for the SNWDP, is one of the most important protection

areas in the country. Therefore, the protection of water quality in the Danjiangkou Reservoir is of extreme importance [2]. In recent years, the reservoir area has adjusted the surrounding agricultural planting structure, reduced industrial waste, and enhanced soil and water conservation, and thus the good water quality of the reservoir has been well maintained at above Class II all year round [3]. However, with the continuous economic development around the reservoir area, many towns have developed aquaculture, Chinese medicinal material processing industries, and forest product processing industries in the mountainous area. Since less construction land restricts the economic development, the land in some areas is over-exploited, leading to destruction of the ecological environment and serious soil erosion, which poses a certain threat to the water quality of the Danjiangkou Reservoir. The water quality of the Danjiangkou Reservoir is not only a problem of water pollution and ecological environment in the reservoir area, but also directly relates to the economic development of large- and medium-sized cities along the middle route of the SNWDP, as well as the safety of residential water use.

The traditional water quality monitoring method mainly used in situ measurements and collection of water samples is used for subsequent laboratory analyses to evaluate water quality [4]. While such measurements are accurate for a point in time and space, they cannot give either the spatial or temporal view of water quality required for the accurate assessment. Consequently, it has certain limitations and cannot achieve real-time monitoring for water quality [5,6]. In recent years, with the continuous development of remote sensing technology, the remote sensing technology in monitoring water quality has served as a non-traditional monitoring technology, which has a wide range of monitoring and can quickly monitor the lake water quality distribution at temporal and spatial scales in real-time, as well as reflect the main sources of pollutants. Meanwhile, remote sensing for water quality monitoring could also predict the flow trend of pollutants, and meet the requirements of spatial and temporal monitoring of water quality in a large-scale water body [7]. The conventional inversion methods of remote sensing water quality parameters mainly include empirical, semi-empirical, and semi-analytical methods [8–10]. Among these methods, the utilization of hyperspectral remote-sensing technology in monitoring water quality has accelerated the advancement of the semi-empirical method. The principle of the semi-empirical method is to perform inversion of water quality parameters via the statistical analyses between the known water quality parameters and the optimal characteristic bands or band combinations, which is currently the most commonly used method for inversion of water quality [11,12]. For instance, Jamil Amanollahi et al. have performed inversion of the water quality variables including pH, total suspended solids (TSS), total dissolved solids (TDS), turbidity, nitrate, sulfate, phosphate, chloride, and the concentration of chlorophyll- $\alpha$  (Chl- $\alpha$ ) in Zarivar International Wetland of Iran using Landsat spectral data and artificial neural network (ANN) models [13]. Yirgalem et al. have developed the neural network model using Landsat spectral data as a proxy to quantify water quality parameters, namely chlorophyll- $\alpha$ , turbidity, and phosphorous in the greater Florida Everglades during the wet and dry seasons [14]. Tian et al. have built the bio-optical model to retrieve the concentrations of tripton, Chl- $\alpha$ , and colored dissolve organic matter (CDOM) of summer Guanting water, and thus obtained the water quality parameters in large-scale water bodies and conducted spatial analysis of water quality [15]. Bresciani et al. have used Landsat 8 OLI(Operational Land Imager) and Sentinel-2A to retrieve the total suspended solids (TSS) and chlorophyll- $\alpha$  concentration and their spatial distribution on lake water quality parameters for the five largest Italian subalpine lakes [16]. Mohamed Elhag et al. have extracted chlorophyll- $\alpha$  concentration, nitrate concentration, and water turbidity in the dam lake of Wadi Baysh, Saudi Arabia using remote sensing data collected from Sentinel-2.

Since some of water quality parameters are not optically active or lack hyperspectral data at fine spatial resolutions, not all parameters can be directly measured by current satellites, including total nitrogen and phosphorus and dissolved oxygen levels. The two key nutrients that drive both green algae and blue-green algae blooms are nitrogen (N) and phosphorus (P). These two nutrients do not impact the visible spectrum of the water body directly but do affect the color due to their promotion of algae growth. While the association between these nutrients and algae growth (i.e., as

represented by Chl-a measurements) may be strong, less is known about the correlations at temporally and spatially smaller samplings [17]. Furthermore, the correlation between N or P and algae growth is based on the fact that one of these nutrients is often considered as the growth limiting factor for an algae bloom. Thus, for one water body the correlation with Chl-a might be with N while for another water body the correlation might be with P, depending on which is the growth limiting factor in that particular water body. Dissolved oxygen (DO) is another important water quality parameter that cannot be directly measured using spectral methods. The main sources of DO in water are atmospheric oxygen transferred into the water column, and oxygen generated in situ due to photosynthesis from algae and other organisms. For remote sensing, indirect methods can be used for detecting dissolved oxygen. Specifically, dissolved oxygen could be impacted by Chl-a and algae in complex ways, such as generation during photosynthesis, consumption during respiration, and by the environmental temperature through solubility, which thus provide indirect diurnal spectral linkages between these parameters.

The total amount of nitrogen (N) on the earth ranks fourth among many elements, which plays a vital role in biological life activities [18]. There are three forms of nitrogen in the ecosystem, namely organic nitrogen, inorganic nitrogen, and molecular nitrogen [19]. The biogeochemical cycle of nitrogen is formed by the mutual transformation of these three forms in the atmosphere, water, and soil. Inorganic nitrogen accounts for a small proportion of soil nitrogen, but it is the main form of nitrogen absorbed by plants, especially nitrate nitrogen and ammonium nitrogen. Currently, irrational fertilizer and the indiscriminate discharge of industrial and municipal wastewater have given rise to the continuous increase of inorganic nitrogen (ammonium nitrogen, nitrate nitrogen, and nitrite nitrogen) in water and soil, which can harm the health of the ecosystem [20]. In order to effectively control the spread of nitrogen pollution and the deterioration of the corresponding pollution, it is crucial to determine the regional pollution sources. Therefore, understanding the transformation mechanism of nitrogen in each environment is of great significance for identification of pollution sources and analysis of pollution process. Under natural conditions, inorganic nitrogen compounds can be transformed into each other in the metabolism of plankton and bacteria. In addition, at a certain temperature, when the  $\text{NH}_3\text{-N}$  concentration changes within a certain range, the average rate of nitrification will also increase with increasing  $\text{NH}_3\text{-N}$  concentration. Nitrogen is also an important factor that causes eutrophication of water bodies and affects algal boom, and thus has a significant impact on water quality [21]. Monitoring the N concentration in the water body is critical to prevent nitrogen pollution and strengthen the ecological environment management of lake water [22]. Total nitrogen (TN) and ammonia nitrogen ( $\text{NH}_3\text{-N}$ ) reflect two important indicators of the nitrogen concentration for water quality. Large-scale reservoirs have a complex composition of water body and exhibit great differences in spatial scales. Even in the same lake or reservoir, the concentrations of TN and  $\text{NH}_3\text{-N}$  are different in different periods [23]. With the assistance of remote sensing technology to quantitatively retrieve TN and  $\text{NH}_3\text{-N}$ , concentrations in reservoirs can clarify the temporal and spatial distribution characteristic, migration, and conversion of TN and  $\text{NH}_3\text{-N}$  in the reservoir area and realize tracing back to the pollution source. For example, Dewidar et al. have developed correlation and regression models between each of the water quality parameters of TN and total phosphorous (TP) at Manzala lagoon, namely the largest brackish water body in the Mediterranean delta coast of Egypt and Thematic Mapper (TM) radiance data. The result indicated that some water quality parameters of TN and TP were significantly correlated with TM radiance data [24]. Kazuo Oki et al. have produced two advanced maps of the potential annual total nitrogen load (PTNL) index and the potential annual total nitrogen load for each river basin area (PTNL/area) index by considering the relationship between the land cover types and the annual total nitrogen load discharged from river basins in the typical urban areas of Japan [25]. Yan et al. have adopted a single factor pollution index and comprehensive pollution index to explore main water pollutants and evaluate water quality pollution level based on the TN inversion results of the Honghe River watershed of China, and have acquired the visualization of the spatial pollution characteristics and identification of potential polluted

risky regions. Banglong Pan et al. have established a quantitative inversion models of total nitrogen (TN) through analyzing a correlation between TN in the Chaohu lake and different bands using HSI (Hyper-Spectrum Image) remote sensing data of HJ-1A satellite [26]. Aiping Feng et al. have been driven by the MODIS (Moderate-resolution Imaging Spectroradiometer) data and used diffuse pollution estimation with remote sensing (DPeRS) to analyze the spatial characteristic of nitrogen diffuse pollution in the Haihe River basin on a pixel scale in 2016 [27]. Liu et al. have established the particle swarm optimization support vector machine (PSO-SVM) model based on the sensitive bands to quantitatively estimate the total nitrogen concentration in surface water of the selected main three rivers in the Ebinur Lake watershed, located in Xinjiang, China to subsequently verify the inversion accuracy of the PSO-SVM model.

The temporal and spatial resolution of different remote sensing sensors and revisit time affect the accuracy of remote sensing inversion of water quality in a certain degree. Sentinel-2 is superior to Landsat 8 OLI in extracting suspended solids in black lakes [28]. The earlier research on water quality remote sensing inversion commonly used remote sensing data include MODIS, HJ-1, Landsat TM/OLI, MERIS (Medium Resolution Imaging Spectrometer), and GF-1 WFV (Wide Field of View). However, the spatial resolution of some satellite data that was relatively low was only suitable for small-scale typical areas, and thus there were limitations in remote sensing inversion of TN and NH<sub>3</sub>-N concentrations in large lakes. Sentinel-2 image is a new generation of multispectral image, equipped with MSI (Multispectral Image) sensor that includes 13 bands, and the relevant revisit time is five days. The Sentinel-2 spatial resolution of the visible light to near-infrared band is 10 m, and the spatial resolution of four red-side bands and two short-wave infrared bands is 20 m. Sentinel-2 integrates the advantages of other satellite remote sensing data, which has the characteristics of short revisit time, high resolution, and strong spectral recognition ability, is suitable for monitoring water of large lakes and ensures more accurate results [29].

The current research mainly focuses on remote sensing inversion of water quality parameters such as chlorophyll- $\alpha$ , water turbidity, total suspended solids (TSS), chemical oxygen demand (COD) in lakes or large reservoirs, while TN and NH<sub>3</sub>-N cannot be directly measured by spectroscopy due to their weak optical characteristics and low signal-to-noise ratio [30]. Therefore, there is little research on remote sensing inversion of TN and NH<sub>3</sub>-N and their spatial distribution and temporal variation. In this study, based on the real-time monitoring data and remote sensing analyses on Sentinel-2 images of the Danjiangkou Reservoir, the sensitive bands of TN and NH<sub>3</sub>-N concentrations were analyzed and a remote sensing inversion model was constructed to retrieve the concentrations of TN and NH<sub>3</sub>-N of the Danjiangkou Reservoir in 2016, 2018, and 2020. Moreover, the temporal and spatial characteristics of TN and NH<sub>3</sub>-N were analyzed, the pollution load of the river basin was revealed, and the sources of pollutants were analyzed, which could provide a scientific reference for water quality monitoring and diffuse pollution control of the Danjiangkou Reservoir.

## 2. Study Area and Data Processing

### 2.1. Study Area

The Danjiangkou Reservoir, as the water source of the middle route of the SNWDP, is located at the junction of Henan, Hubei, and Shaanxi and at 0.8 km downstream the junction of the Danjiang River and Hanjiang River. Hence, the Danjiangkou Reservoir can be subdivided into the Han Reservoir and Dan Reservoir. The water source for the middle route of the SNWDP is mainly located in the Danjiang Reservoir area, and the water source mainly comes from the Danjiang River basin that flows through the Shaanxi and Henan provinces (Figure 1). The gate for the water diversion canal is located at Taocha in Xichuang County, Nanyang City, Henan Province. In 2013, the height of the Danjiangkou Dam was increased to 176.6 m, with a total area of about 300 km<sup>2</sup>. Due to the river cut, most of the landform of the reservoir is massive mountainous forest, and the topography fluctuates greatly. The Danjiangkou Reservoir lies within the northern subtropical zone, and the region exhibits a subtropical

monsoon climate. The annual precipitation is 804.3 mm and the average annual air temperature is 15.8 °C. In recent years, the focus has been on the development of characteristic forest and fruit industries such as honeysuckle, walnut, and kiwi, as well as the promotion of bio-organic fertilizers and low- and non-toxic pesticides in the reservoir area and its surrounding areas. On the one hand, the above measures can prevent the loss of nitrogen and phosphorus in the soil. On the other hand, these measures can stabilize soil and preserve water.

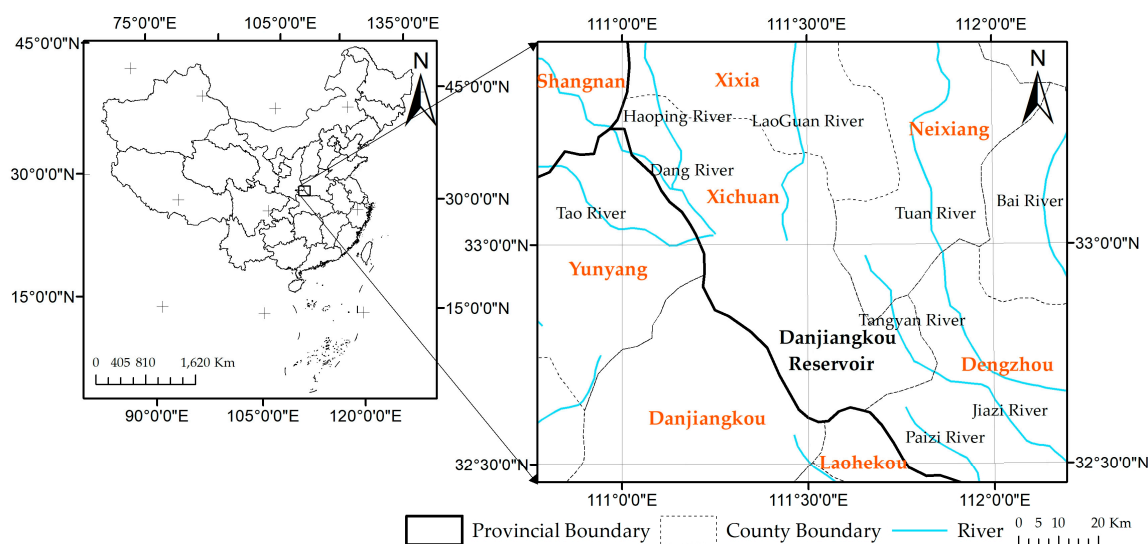


**Figure 1.** Regional location of the water source for the middle route of the South-to-North Water Diversion Project (SNWDP).

## 2.2. Data Processing

### 2.2.1. Water Quality Monitoring Section and Data Acquisition

This work took the water quality parameters total nitrogen (TN) and ammonia nitrogen ( $\text{NH}_3\text{-N}$ ) as the research object, and relied on the automatic monitoring station that has been built by the Danjiangkou Reservoir Headway Management Bureau. In February 2016 and February 2020, the water quality monitoring data of a total of 70 sampling sites in the Danjiangkou Reservoir were collected. Among them, the water quality data of 2016 were used for sensitive band analysis and the construction of inversion models, and the water quality data of 2020 were used for accuracy verification (Figure 2). All water quality data of 70 sampling sites were collected by GPS (Global Positioning System) navigation. In the laboratory, a water sample of 0.5 m from the surface was collected with a plexiglass water collector, and the water sample was stored in an incubator at 2–8 °C, which was tested and analyzed within 48 h. Half of the original water was measured for TN, another half original water was filtered by 0.45  $\mu\text{m}$  mixed fiber membrane, and the filtrate was used to measure  $\text{NH}_3\text{-N}$ . TN was measured by alkaline potassium persulfate oxidation-spectrophotometry, and  $\text{NH}_3\text{-N}$  was measured by Nessler's reagent photometric method. Statistics of the measure results were shown in Table 1.

**Table 1.** Statistics of the measured results.

|                        | Year | Max                                 | Min                                 | Mean                                | Standard Error |
|------------------------|------|-------------------------------------|-------------------------------------|-------------------------------------|----------------|
| TN                     | 2016 | 1.230 $\text{mg}\cdot\text{L}^{-1}$ | 0.820 $\text{mg}\cdot\text{L}^{-1}$ | 1.022 $\text{mg}\cdot\text{L}^{-1}$ | 0.097          |
|                        | 2020 | 1.174 $\text{mg}\cdot\text{L}^{-1}$ | 0.693 $\text{mg}\cdot\text{L}^{-1}$ | 0.928 $\text{mg}\cdot\text{L}^{-1}$ | 0.106          |
| $\text{NH}_3\text{-N}$ | 2016 | 0.07 $\text{mg}\cdot\text{L}^{-1}$  | 0.002 $\text{mg}\cdot\text{L}^{-1}$ | 0.025 $\text{mg}\cdot\text{L}^{-1}$ | 0.002          |
|                        | 2020 | 0.059 $\text{mg}\cdot\text{L}^{-1}$ | 0.001 $\text{mg}\cdot\text{L}^{-1}$ | 0.017 $\text{mg}\cdot\text{L}^{-1}$ | 0.001          |

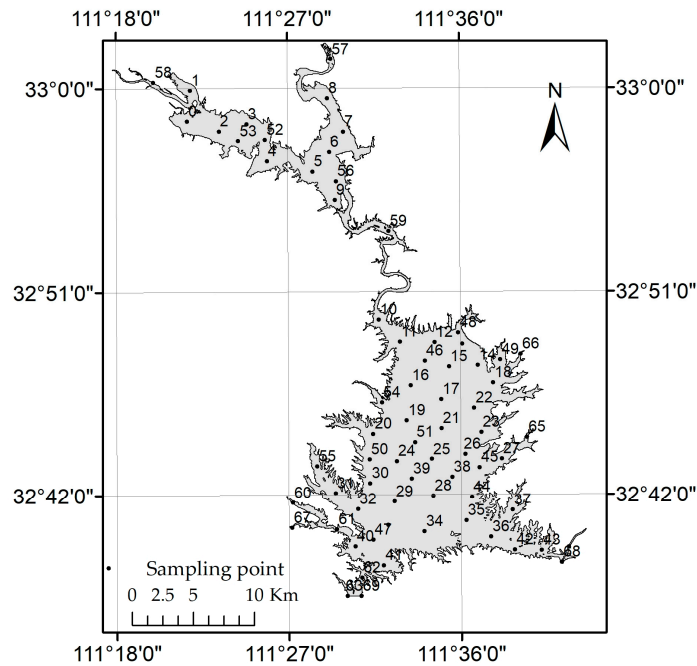


Figure 2. Distribution of the sample sites for water quality monitoring.

2.2.2. Remote Sensing Image Data Collection and Preliminary Processing

In this study, Sentinel-2 was selected as the image data, and the water quality monitoring data were selected for the same time and month, that is, February 16, 2016 (Sentinel-2A), 11 March 2018 (Sentinel-2A), and 12 March 2020 (Sentinel-2B), considering the cloudy coverage of less than 5% for these three sceneries. The atmospheric correction and radiometric calibration on all images were performed by using Sen2cor plugin in SNAP (Sentinels Application Platform). The modified normalized difference water index (MNDWI) was calculated for the images processed by atmospheric correction and radiometric calibration, and the information of the water body of the Danjiangkou Reservoir was retrieved through the statistical function of masking; the results are shown in Figure 3. Finally, the normalized difference vegetation index (NDVI) was used to eliminate the distribution area of aquatic vegetation, to obtain the remote sensing reflectance image of the water body without aquatic vegetation coverage.

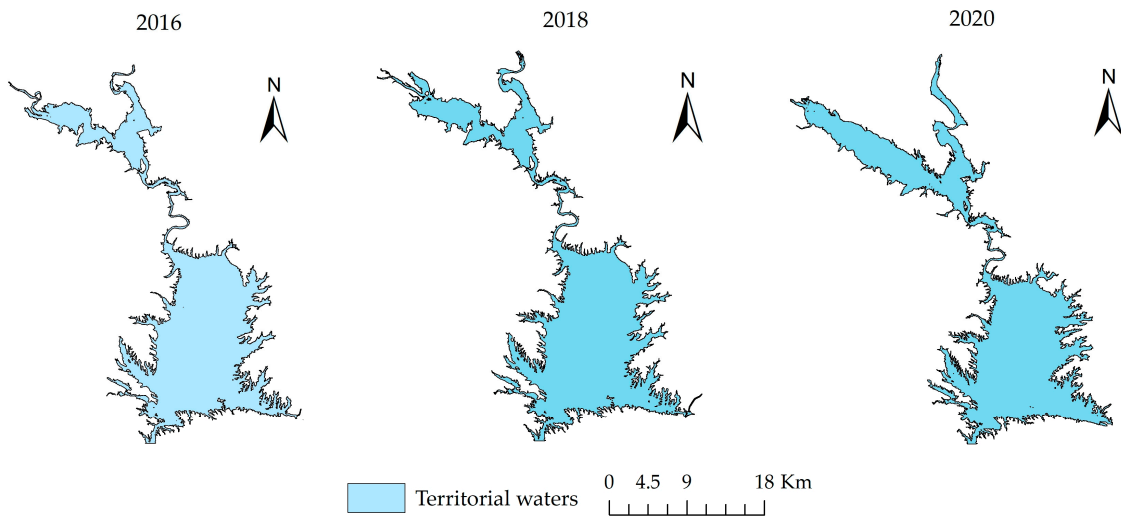
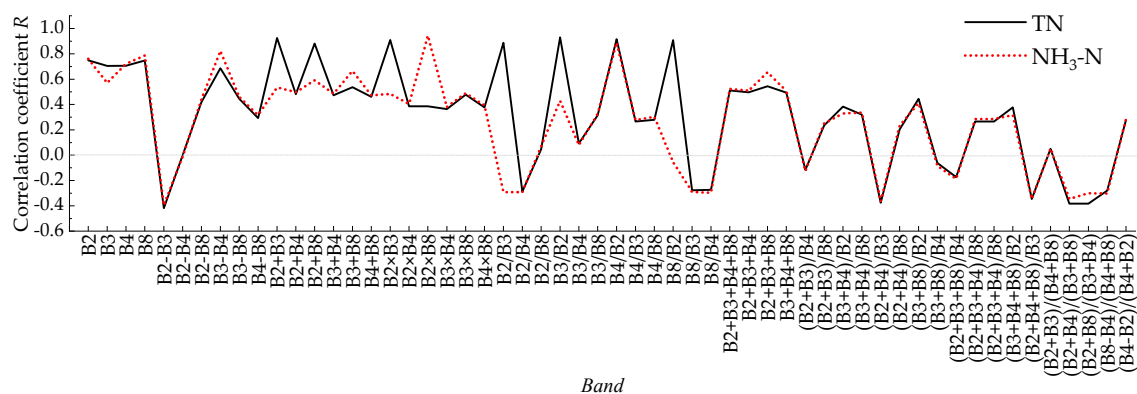


Figure 3. The water area map of the Danjiangkou Reservoir in 2016, 2018, and 2020.

### 3. Sensitive Bands Analysis of TN and NH<sub>3</sub>-N Concentrations

Substances in surface water can significantly change the backscattering characteristics of light. The remote sensing technology for monitoring water quality relies on the changes in the spectral characteristics of backscattering and correlates the spectral changes with water quality parameters through analytical models [31]. The optimal wavelength for evaluating the quality index mainly depends on the concentration of the water quality parameters and the characteristics of the sensor [32]. This study first used the measured TN and NH<sub>3</sub>-N data in 2016 to perform Pearson correlation analysis with all the bands of Sentinel-2 images. The results showed that Sentinel-2 had a positive association with TN and NH<sub>3</sub>-N in each band. Among them, B2 blue band (0.490 nm), B3 green band (0.560 nm), B4 red band (0.665 nm), and B8 near infrared band (0.842 nm) had a strong association with the concentration of TN and NH<sub>3</sub>-N. In this study, the remote sensing reflectance of the four bands of B2, B3, B4, and B8 in the form of single band, band summation, and other different band combinations were performed during the correlation analysis with the measured TN and NH<sub>3</sub>-N data; the results are shown in Figure 4.



**Figure 4.** Correlation coefficients of different band combinations. TN, total nitrogen.

In Figure 4, among 56 different band combinations, the correlation coefficient between B2 × B8 and the measured TN concentration was 0.9301, which was the highest among all band combinations. The correlation coefficient between B3/B2 and the measured NH<sub>3</sub>-N concentration was 0.9444, which was the highest among all band combinations. Therefore, two band combinations of B2 × B8 and B3/B2 were selected as the factors for constructing the inversion model of the TN and NH<sub>3</sub>-N concentration of the Danjiangkou Reservoir.

### 4. The Inversion Model of TN and NH<sub>3</sub>-N Concentrations

Taking the two band combination indexes of B2 × B8 and B3/B2 as independent variables, and the measured TN and NH<sub>3</sub>-N concentrations as dependent variables, the corresponding functional relationships were established through statistical methods to construct remote sensing inversion models for TN and NH<sub>3</sub>-N concentrations. Based on the data of 70 sampling sites measured in 2016, four types of trend prediction and regression analysis including linear, quadratic polynomial, logarithmic, and power function were used to establish remote sensing inversion models of TN and NH<sub>3</sub>-N concentrations. The relationship between the band combination and the concentration of TN and NH<sub>3</sub>-N was obtained by fitting, as shown in Table 2. It can be seen from Table 1 that the quadratic polynomial model had the highest fitting accuracy in the concentrations of TN and NH<sub>3</sub>-N, and their R<sup>2</sup> was 0.782 and 0.851, respectively (Table 2). The measured concentrations of TN and NH<sub>3</sub>-N at 70 sampling sites in February 2020 were subjected to quadratic polynomial regression with the concentrations of TN and NH<sub>3</sub>-N predicted by the model to verify the model accuracy in predicting the concentrations of TN and NH<sub>3</sub>-N. Linear relationship between the measured and the predicted concentrations of NH<sub>3</sub>-N and TN are respectively shown in Figure 5a,b.

**Table 2.** The relationship between the band combination and the concentration of TN and NH<sub>3</sub>-N.

|                    | Band Combination | Model                            | R <sup>2</sup> | MAE    | RMSE   |
|--------------------|------------------|----------------------------------|----------------|--------|--------|
| TN                 | B2 × B8          | $y = 0.114x + 0.843$             | 0.748          | 0.0959 | 0.085  |
|                    |                  | $y = -0.194x^2 + 1.962x - 1.955$ | 0.783          | 0.0887 | 0.079  |
|                    |                  | $y = 0.507 + 0.777 \ln(x)$       | 0.772          | 0.0923 | 0.091  |
|                    |                  | $y = 0.907 + x^{1.215}$          | 0.728          | 0.0906 | 0.83   |
| NH <sub>3</sub> -N | B3/B2            | $y = 0.474x + 0.276$             | 0.739          | 0.0079 | 0.0107 |
|                    |                  | $y = 0.296x^2 - 0.224x - 0.328$  | 0.851          | 0.0091 | 0.0099 |
|                    |                  | $y = 1.585 + 0.369 \ln(x)$       | 0.759          | 0.0085 | 0.0083 |
|                    |                  | $y = -2.601 + 2.948x^{0.351}$    | 0.746          | 0.0081 | 0.0091 |

Note: RMSE is Root Mean Square Error MAE is Mean Absolute Error.

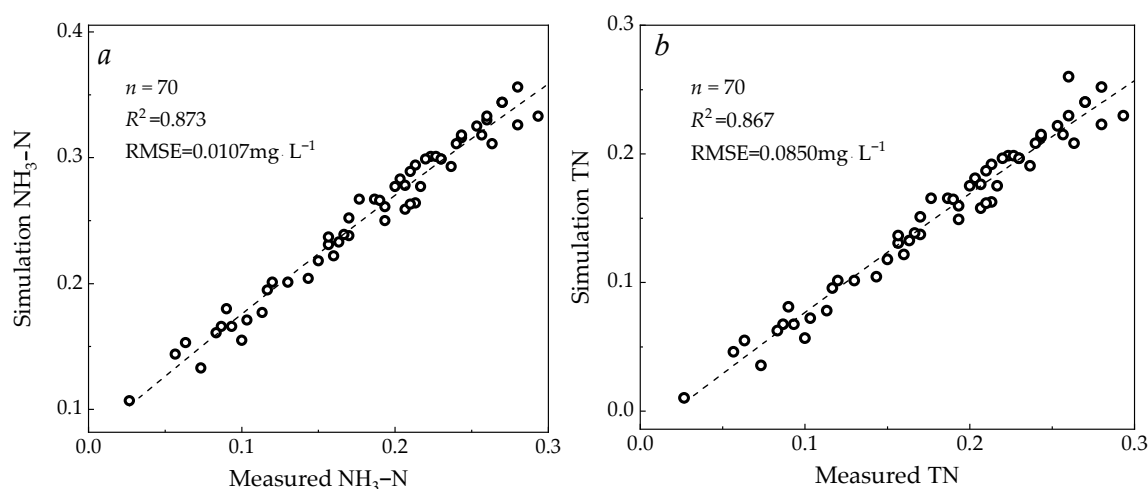


**Figure 5.** Accuracy of linear relationship between predicted and measured concentrations of NH<sub>3</sub>-N (a) and TN (b). RMSE, root mean square error.

From Figure 5a,b, there was a good linear relationship between the measured and the predicted concentrations of TN and NH<sub>3</sub>-N. The R<sup>2</sup> was 0.873 for TN and 0.867 for NH<sub>3</sub>-N, respectively, and the corresponding root mean square error (RMSE) was 0.0107 mg·L<sup>-1</sup> and 0.0850 mg·L<sup>-1</sup>, which indicated that the constructed inversion model had high prediction accuracy and was suitable for remote sensing inversion of TN and NH<sub>3</sub>-N concentrations in the reservoir area of Sentinel-2 images.

The spatial distribution of predicted and measured concentrations of TN and NH<sub>3</sub>-N of all the 70 observation points are shown in Figure 6. From Figure 6, the difference between the maximum TN measured value and predicted value was 0.068 mg·L<sup>-1</sup>, and minimum was 0.101 mg·L<sup>-1</sup>; the difference between the maximum NH<sub>3</sub>-N measured value and predicted value was 0.009 mg·L<sup>-1</sup> and the minimum was 0.0001 mg·L<sup>-1</sup>. It can be seen that the difference between the measured value and the model predicted value was small. The measured value was in accordance with the model predicted value in spatial distribution and there was no significant difference. The analysis also indicated that the constructed inversion model had high prediction accuracy and was suitable for remote sensing inversion of TN and NH<sub>3</sub>-N concentrations in the reservoir area of Sentinel-2 images.

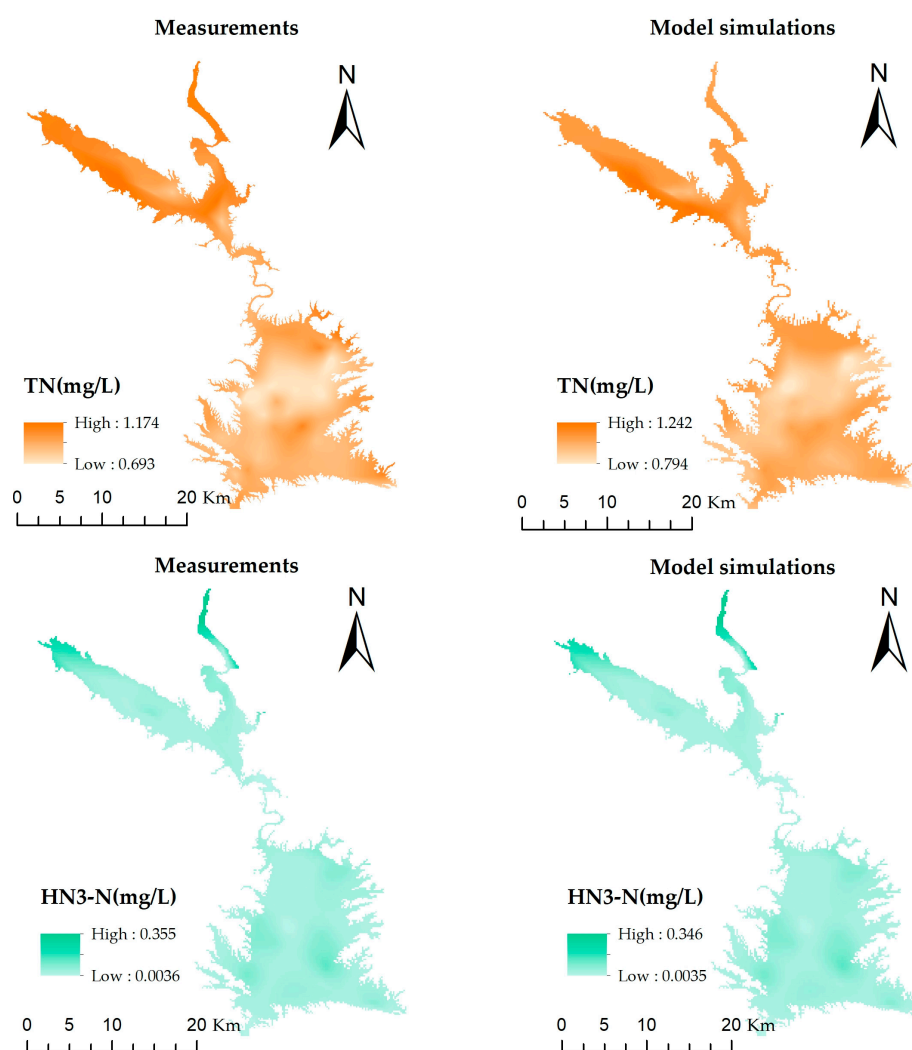


**Figure 6.** The spatial distribution of TN and  $\text{NH}_3\text{-N}$  predicted and measured concentrations of all 70 observation points.

## 5. Analysis of TN and $\text{NH}_3\text{-N}$ Change Characteristics in the Reservoir Area of the Water Source Area of the Middle Route of the SNWDP

This study used the established remote sensing inversion model for the TN and  $\text{NH}_3\text{-N}$  concentrations on the spatial grid scale, combined with the concentration of TN and  $\text{NH}_3\text{-N}$  in 2016, to retrieve the remote sensing images of the Danjiangkou Reservoir in 2018 and 2020, and further estimate the concentration of TN and  $\text{NH}_3\text{-N}$  to reveal the spatial differentiation and variation characteristic of TN and  $\text{NH}_3\text{-N}$ . The results are shown in Table 3 and Figure 7.

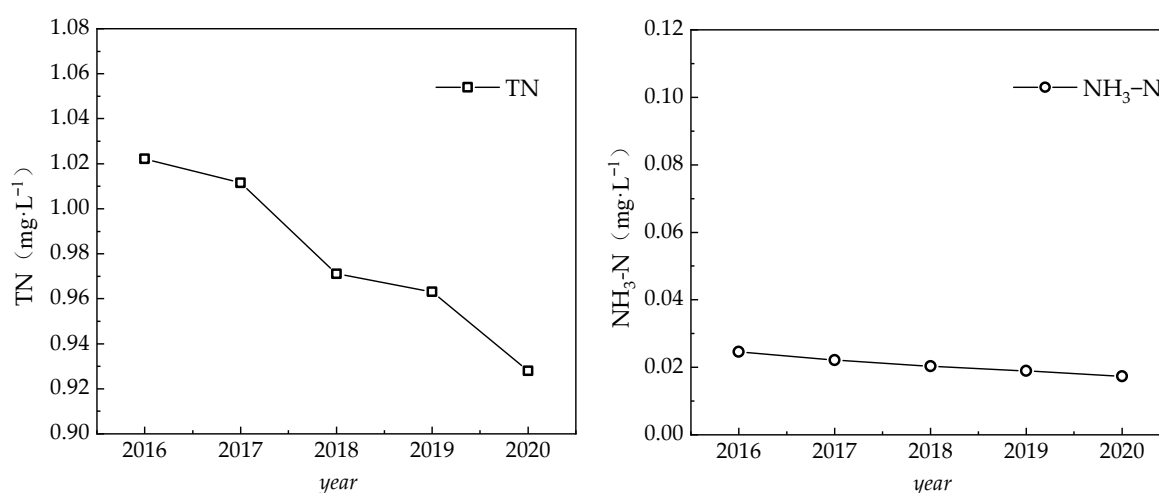
### 5.1. Inter-Annual Variation Characteristic of TN and $\text{NH}_3\text{-N}$ Concentrations

The results in Figure 7 show that the annual averages of TN and  $\text{NH}_3\text{-N}$  during the study period did not fluctuate, and both demonstrated a downward trend. Among them, the TN concentration has a large downward trend, from  $1.02 \text{ mg}\cdot\text{L}^{-1}$  in 2016 to  $0.928 \text{ mg}\cdot\text{L}^{-1}$  in 2020; while the  $\text{NH}_3\text{-N}$  concentration has a relatively flat downward trend from  $0.0246 \text{ mg}\cdot\text{L}^{-1}$  in 2016 to  $0.0173 \text{ mg}\cdot\text{L}^{-1}$  in 2020.

**Table 3.** Changes of TN and NH<sub>3</sub>-N concentrations during the study period.

| Year | Parameter          | Water Quality Classification |          |           |          |         | Minimum<br>mg·L <sup>-1</sup> | Maximum<br>mg·L <sup>-1</sup> |
|------|--------------------|------------------------------|----------|-----------|----------|---------|-------------------------------|-------------------------------|
|      |                    | Class I                      | Class II | Class III | Class IV | Class V |                               |                               |
| 2016 | TN                 | 0                            | 0        | 41.3%     | 58.7%    | 0       | 0.820                         | 1.230                         |
| 2018 |                    | 0                            | 0        | 70.68%    | 29.32%   | 0       | 0.747                         | 1.204                         |
| 2020 |                    | 0                            | 0        | 73.49%    | 26.51%   | 0       | 0.369                         | 1.174                         |
| 2016 | NH <sub>3</sub> -N | 100%                         | 0        | 0         | 0        | 0       | 0.002                         | 0.067                         |
| 2018 |                    | 100%                         | 0        | 0         | 0        | 0       | 0.0014                        | 0.061                         |
| 2020 |                    | 100%                         | 0        | 0         | 0        | 0       | 0.0009                        | 0.0596                        |

Note: According to environmental quality standards for surface water of China (GB3838-2002) [33]. The TN classification standard is: Class I (0–0.2), Class II (0.2–0.5), Class III (0.5–1), Class IV (1–1.5), Class V (1.5–2.0); The NH<sub>3</sub>-N classification standard is: Class I (0–0.15), Class II (0.15–0.5), Class III (0.5–1), Class IV (1–1.5), and Class V (1.5–2.0).

**Figure 7.** Accuracy of linear relationship between predicted and measured TN and NH<sub>3</sub>-N concentrations.

The results in Table 3 show that the minimum concentrations of NH<sub>3</sub>-N in 2016, 2018, and 2020 were 0.002, 0.0014, and 0.0009 mg·L<sup>-1</sup>, respectively, and the maximum concentrations were 0.067<sup>1</sup>, 0.061, and 0.0596 mg·L<sup>-1</sup>, respectively, which meet Class II (Table 3). The minimum TN concentrations in 2016, 2018, and 2020 were 0.820, 0.747, and 0.369 mg·L<sup>-1</sup>, respectively, and the maximum concentrations were 1.230, 1.204, and 1.174 mg·L<sup>-1</sup>, respectively. Among them, the maximum concentrations of 0.067 mg·L<sup>-1</sup> for NH<sub>3</sub>-N was less than 0.15 mg·L<sup>-1</sup>, which has already met the requirements of Class I in the national environmental quality standards for surface water. After TN was involved in the water quality assessment of the reservoir area, the maximum concentration of 1.174 mg·L<sup>-1</sup> was less than 1.5 mg·L<sup>-1</sup>, which could basically meet Class IV. In terms of the area of TN and NH<sub>3</sub>-N in total water bodies, the area covered by TN Class III has increased from 41.3% in 2016 to 73.49% in 2020, and the area covered by Class IV has dropped from 58.7% in 2016 to 26.51% in 2020.

### 5.2. Spatial Variation Characteristic of TN and NH<sub>3</sub>-N Concentrations

According to the inversion results of TN and NH<sub>3</sub>-N, the spatial distribution of TN and NH<sub>3</sub>-N concentrations in the Danjiangkou Reservoir in different years were obtained (Figure 8). According to the section line of TN and NH<sub>3</sub>-N concentrations set in this study, a longitudinal section of TN and NH<sub>3</sub>-N concentrations was drawn (Figure 8). In this way, the variation characteristic of the temporal and spatial distribution of TN and NH<sub>3</sub>-N concentrations were analyzed, and the trend of pollutants variation and major pollution sources were explored.

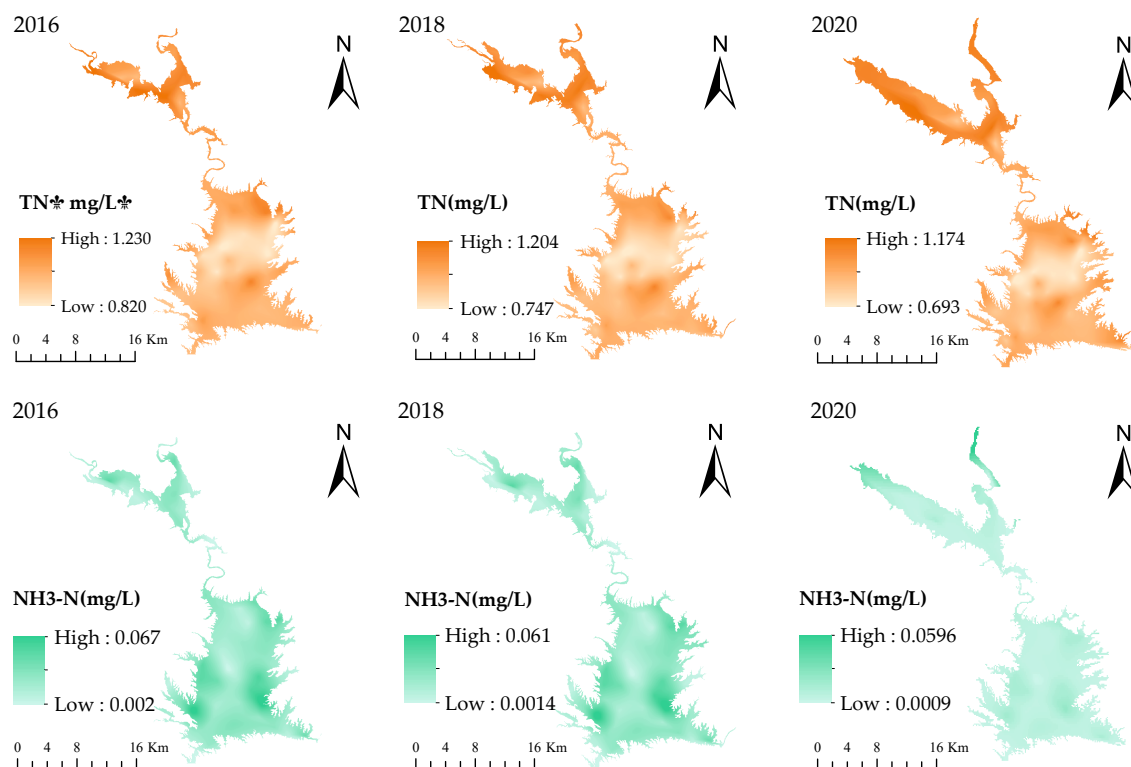


**Figure 8.** Temporal and spatial distribution characteristics of TN and  $\text{NH}_3\text{-N}$  concentrations during the study period.

As indicated in Figure 8, the concentrations of TN and  $\text{NH}_3\text{-N}$  showed some concentrated areas centered on points and planes, but showed an expanding trend in the water areas where the concentration decreased. In the Danjiang River basin and the area at the entrance of the reservoir and some areas in the middle of the reservoir area, the concentration of TN was mainly concentrated between  $1 \text{ mg}\cdot\text{L}^{-1}$  and  $1.174 \text{ mg}\cdot\text{L}^{-1}$ , which was higher than other areas in the reservoir area and these areas had expanded in 2018. The concentration of  $\text{NH}_3\text{-N}$  with a higher concentration was between  $0.03 \text{ mg}\cdot\text{L}^{-1}$  and  $0.0596 \text{ mg}\cdot\text{L}^{-1}$ , generally increasing from the middle to the east and west sides, and the marginal areas on the east and west sides of the southern part of the reservoir area were always in the areas with higher concentrations of  $\text{NH}_3\text{-N}$ , showing a planar concentration trend. The concentration of  $\text{NH}_3\text{-N}$  in this area in 2020 decreased dramatically and the area was further reduced, while the area with a high concentration of  $\text{NH}_3\text{-N}$  at the front end of the Danjiang River basin expanded to a certain extent by 2020.

## 6. Discussion

Nitrogen causes eutrophication of water bodies and the main sources of nitrogen include three aspects: soil nutrients, decomposition of plant residues, and external input [34]. This study discovered that the main sources of TN and  $\text{NH}_3\text{-N}$  concentrations in the Danjiangkou Reservoir were soil nutrients and external input. During the study period, the concentrations of TN and  $\text{NH}_3\text{-N}$  of the reservoir demonstrated an overall downward trend, indicating that the water quality of the Danjiangkou Reservoir had continuous improvements. The measures to enhance agricultural non-point source pollution control and ecological construction along the water source area have made significant progress.

Regarding the temporal changes of TN and  $\text{NH}_3\text{-N}$  concentrations, there were no major fluctuations in the concentrations of TN and  $\text{NH}_3\text{-N}$  of the Danjiangkou Reservoir from 2016 to 2020, and both the minimum and maximum concentrations showed a downward trend. During the study period, the concentration of  $\text{NH}_3\text{-N}$  has been in line with Class I, and the concentration was relatively small in Class I, and the water quality was good, while the TN concentration was between Class III and Class

IV. Generally, the Danjiangkou Reservoir had good water quality from 2016 to 2020. The inter-annual variation indicated that the water quality parameters TN and  $\text{NH}_3\text{-N}$  of the reservoir have shown a downward trend, and the water quality has shown an overall upward trend. Pertaining to the spatial variation of TN and  $\text{NH}_3\text{-N}$  concentrations, the concentration of TN was higher in some areas in the middle of the reservoir area. This research selected the water quality data for the dry season in February. During this period, a detention water body and a small lake with a lower water level formed in the middle of the reservoir area. The bottom of the water body at the center of the lake tended to be agitated, causing sedimentary pollutants to suspend to the lake surface and release nitrogen. Therefore, the concentration of TN was significantly higher in some areas of the middle of the reservoir area. Yuanyuan Zhu et al. have pointed out that among the 10 main rivers entering the Danjiangkou Reservoir, the Han River has the largest TN input, followed by the Duhe River and Laoguan River. Zhongyuan Li et al. have found that the pollutant yield of the Guanhe River was the most, followed by the Danjiang River, Qihe River, and Taohe River. The Danjiang River, Laoguan River, and Tao River were the main tributaries that enter the northern part of the Danjiangkou Reservoir. Although the Danjiang River, Tao River, and Laoguan River entering the reservoir and the tributaries around the reservoir were relatively small, their TN load was relatively high. After entering the reservoir, the flow velocity decreased and thus the nitrogen elements tended to accumulate at the entrance, which was consistent with the areas with a high TN concentration mainly concentrated in the area at the entrance of the river in this study. This further confirmed that the temporal and spatial variation of water quality were caused by processes such as resuspension of suspended sediments and point source inflow of nutrients on a smaller spatial scale. The area with a high concentration of  $\text{NH}_3\text{-N}$  was located on the east and west edges of the southern part of the reservoir area, showing a trend of the planar concentration. This is because the surrounding terrain of the above-mentioned area was complex and the big slope and drop had a weak protection against soil erosion. Once soil erosion occurred, the chemical fertilizer carried in the lost soil and water was the cause of the high  $\text{NH}_3\text{-N}$  concentration in the water area. Generally, the larger the proportion of residential land and cultivated land in the basin, the higher the concentration of N in the water body [35]. The on-site investigation on the east and west sides of the southern part of the reservoir area showed that the proportion of cultivated land in this area was relatively high. Agriculture was the main production activity in this area. The local residents improperly used pesticides and fertilizers to increase production. The surface runoff carried a large amount of nitrogen into the water body, resulting in a high background value of the nitrogen concentration parameter of the rivers entering the reservoir. Therefore, the concentration of  $\text{NH}_3\text{-N}$  in this region was relatively high.

The contribution rate of  $\text{NH}_3\text{-N}$  played an important role in TN and directly affected the TN concentration. After the state implemented the environmental protection policy of prohibiting phosphorous, nitrogen has been recognized the main control object [36]. Compared with TN,  $\text{NH}_3\text{-N}$  could have a direct impact on the water quality, which is more relevant. The concentration of TN and  $\text{NH}_3\text{-N}$  in the study area did not show consistency in the spatial distribution. By calculating the average concentration of  $\text{NH}_3\text{-N}$  and TN in all sampling sites in 2016, 2018, and 2020, the percentages of  $\text{NH}_3\text{-N}$  in TN in the three periods were 1.43%, 1.22%, and 1.13%, respectively, indicating that nitrogen of other forms in the reservoir area accounted for a large proportion of TN. When the concentration of  $\text{NH}_3\text{-N}$  in the water body was higher than  $2.5 \text{ mg}\cdot\text{L}^{-1}$ , the concentration of TN and the concentration of  $\text{NH}_3\text{-N}$  shows a certain linear correlation [36]. In this study, it was found that the two concentrations did not have a good linear relationship after linear analysis of TN and  $\text{NH}_3\text{-N}$  in 2016, 2018, and 2020, indicating that the concentration of  $\text{NH}_3\text{-N}$  in the reservoir area was relatively low. This could also verify a certain accuracy of the inversion results to a certain degree.

The quadratic polynomial model used in this study has achieved a certain accuracy in the inversion of TN and  $\text{NH}_3\text{-N}$  in the Danjiangkou Reservoir, but there were still some limitations. The application in the area is needed to adjust the model coefficients in order to obtain more accurate results. The band range of Sentinel-2 data in this study could be used for the inversion of TN and  $\text{NH}_3\text{-N}$  in lakes and

reservoirs. However, due to the limited availability of Sentinel-2 data, the most remote sensing images in summer were blocked by clouds and could not be processed. The concentrations of TN and  $\text{NH}_3\text{-N}$  in the wet and dry periods of the reservoir area have not been compared, the effect of plant growth and microorganisms on nitrogen purification could not be characterized, and the relationship between the concentration of TN and  $\text{NH}_3\text{-N}$  in winter and summer could not be well elucidated.

Currently, the remote sensing monitoring of water quality of large lakes still remains in some limited water quality parameters, such as Chl-a, TSS, Transparency, DO, and so on. The measured Chl-a concentration, water quality optical characteristics, and spectral data could establish a high-precision remote sensing inversion model. However, due to the differences in the natural geographic environment and the water environment, the prediction accuracy of these established inversion models for remote sensing monitoring of water quality parameters is not very high. The monitor results still require considerable field verification work. These inversion models are only suitable for macroscopic water quality evaluation, classification, and management (e.g., remote sensing mapping), but cannot replace accurate on-site water quality monitoring procedures. Therefore, the key to promote the practical application of remote sensing inversion of water quality parameters in large lakes is to discover the characteristics of spectral response curves of different water quality parameters. It is also necessary to establish a complete quantitative model library based on different water quality parameters, and thus dynamic monitoring of water quality can be realized by selecting the optimal model in a specific area.

The establishment of the model library can reduce the cost of water quality monitoring, improve work efficiency, and reduce monitoring errors. Moreover, the composition of large lakes is complex, and the spectral information overlaps each other. Therefore, it is reasonable to strengthen the study of the spectral characteristics of each water quality parameter, which helps to reduce the influence of the mixed pixel problem during the monitoring process and improve the inversion accuracy. Ultimately, the true remote sensing data used in water quality monitoring could be acquired.

## 7. Conclusions

Based on Sentinel-2 remote sensing data and ground monitoring water quality data, this study has attained the inversion of two water quality parameters TN and  $\text{NH}_3\text{-N}$  concentrations in the Danjiangkou Reservoir in 2016, 2018, and 2020 by establishing a quadratic polynomial model and the spatio-temporal variation of water quality parameters has been analyzed. The following conclusions have been reached:

The quadratic polynomial inversion models of the band  $\text{B2} \times \text{B8}$  for TN and  $\text{B3/B2}$  for  $\text{NH}_3\text{-N}$  were established using remote sensing reflectance of Sentinel-2 images. Meanwhile, the measured data of TN and  $\text{NH}_3\text{-N}$  were used to verify the accuracy of the inversion values obtained by the model. The results showed that the model could be suitable for remote sensing inversion of TN and  $\text{NH}_3\text{-N}$  concentrations in Sentinel-2 images.

The  $\text{NH}_3\text{-N}$  concentration in the Danjiangkou Reservoir has been in line with Class I from 2016 to 2020, the concentration was relatively smaller in Class I, and the corresponding water quality was pretty good, while the TN concentration was between Class III and Class IV. The inter-annual variation indicated that both TN and  $\text{NH}_3\text{-N}$  concentrations in the reservoirs have shown a downward trend, and the overall water quality had exhibited an upward trend.

During the dry season, a detention area of water body formed in the middle of the reservoir area, and thus a small lake with a low independent water level formed. The bottom of water body at the lake center was easily disturbed, causing sedimentary pollutants to suspend to the lake surface and release nitrogen, resulting in a higher TN concentration. In the northern part of the Danjiangkou Reservoir, the main inflow of the reservoir and the tributaries around the reservoir were relatively small, but the inflow load of TN was relatively large, which made the areas with a high TN concentration at the river entrance. The mountainous areas on the east and west sides of the southern of the Danjiangkou Reservoir had large slopes, which were inclined to soil erosion. The lost soil and carried a large amount of pesticides and fertilizers, and the area had a high proportion of the cultivated land. Moreover,

the pesticides and fertilizers were improperly used by the local residents to increase production. Therefore, the ground runoff carries a large amount of nitrogen into the water body, resulting in a higher background value of the nitrogen concentration indicators of the rivers ultimately entering the reservoir, and increasing the  $\text{NH}_3\text{-N}$  concentration of water bodies on the east and west sides of the reservoir area.

**Author Contributions:** Research conduct and funding acquisition, Z.H.; data processing and analysis, G.D.; manuscript writing, X.L.; model construction and validation, Y.F.; data collection, W.Z. All authors have read and agreed to the published version of the manuscript.

**Funding:** This research has been supported by China University of Mining and Technology-Beijing “Outstanding scholars of YueQi” award project and Henan Province University Science and Technology Innovation Team Support Plan, grant number 18IRTSTHN008 and Henan Polytechnic University Doctoral foundation project, grant number B2017-12.

**Acknowledgments:** We thank the authors and institutions who provided us with these data. We also thank those anonymous reviewers who provide valuable suggestions for the revision of this paper. We appreciate the linguistic assistance provided by TopEdit ([www.topedit.com](http://www.topedit.com)) during the preparation of this manuscript.

**Conflicts of Interest:** The authors declare no conflict of interest.

## References

- Sheng, H.; Zhi, N.X.; Kui, L.J.; Guo, S.D.; Hua, Z. Environmental problems and risk analysis for operation of Middle Route Project of South to North Water Diversion. *Yangtze River* **2019**, *50*, 46–51.
- Fei, G.S.; Ping, G.Y.; Hu, L.; Han, D.W.; Wu, X.N. Characteristics of surface runoff and agricultural non-point source pollution in the core water source area of the Danjiangkou Reservoir. *J. Agro-Environ. Sci.* **2019**, *38*, 2816–2825.
- Qi, W.Z.; Xing, L.X.; Hong, Y.Z.; Guang, Y.L.; Yue, C.; Chu, L.Z.; Hai, C.L. Endogenous Release of Nitrogen and Phosphorus in the Danjiangkou Reservoir. *Environ. Sci.* **2019**, *40*, 4953–4961.
- Gitelson, A.; Garbuzov, G.; Szilagyi, F.; Mittenzwey, K.-H.; Karnieli, A.; Kaiser, A. Quantitative remote sensing methods for real-time monitoring of inland waters quality. *Int. J. Remote Sens.* **1993**, *14*, 1269–1295. [[CrossRef](#)]
- Wang, X.; Yang, W. Water quality monitoring and evaluation using remote sensing techniques in China: A systematic review. *Ecosyst. Health Sustain.* **2019**, *5*, 47–56. [[CrossRef](#)]
- Peletz, R.; Kumpel, E.; Bonham, M.; Rahman, Z.; Khush, R. To What Extent is Drinking Water Tested in Sub-Saharan Africa? A Comparative Analysis of Regulated Water Quality Monitoring. *Int. J. Environ. Res. Public Health* **2016**, *13*, 275. [[CrossRef](#)] [[PubMed](#)]
- Fink, G.; Burke, S.; Simis, S.G.H.; Kangur, K.; Kutser, T.; Mulligan, M. Management Options to Improve Water Quality in Lake Peipsi: Insights from Large Scale Models and Remote Sensing. *Water Resour. Manag.* **2018**, *34*, 1–14. [[CrossRef](#)]
- Caballero, I.; Morris, E.P.; Ruiz, J.; Navarro, G. Assessment of suspended solids in the Guadalquivir estuary using new DEIMOS-1 medium spatial resolution imagery. *Remote Sens. Environ.* **2014**, *146*, 148–158. [[CrossRef](#)]
- Nechad, B.; Ruddick, K.G.; Park, Y. Calibration and validation of a generic multisensor algorithm for mapping of total suspended matter in turbid waters. *Remote Sens. Environ.* **2010**, *114*, 854–866. [[CrossRef](#)]
- Schiller, H.; Doerffer, R. Neural network for emulation of an inverse model operational derivation of Case II water properties from MERIS data. *Int. J. Remote Sens.* **1999**, *20*, 1735–1746. [[CrossRef](#)]
- Doña, C.; Chang, N.-B.; Caselles, V.; Sánchez, J.M.; Camacho, A.; Delegido, J.; Vannah, B.W. Integrated satellite data fusion and mining for monitoring lake water quality status of the Albufera de Valencia in Spain. *J. Environ. Manag.* **2015**, *151*, 416–426. [[CrossRef](#)] [[PubMed](#)]
- Chawira, M.; Dube, T.; Gumindoga, W. Remote sensing based water quality monitoring in Chivero and Manyame lakes of Zimbabwe. *Phys. Chem. Earth Parts A/B/C* **2013**, *66*, 38–44. [[CrossRef](#)]
- Amanollahi, J.; Kaboodvandpour, S.; Majidi, H. Evaluating the accuracy of ANN and LR models to estimate the water quality in Zarivar International Wetland, Iran. *Nat. Hazards* **2016**, *85*, 1511–1527. [[CrossRef](#)]
- Chebud, Y.; Naja, G.M.; Rivero, R.G.; Melesse, A.M. Water Quality Monitoring Using Remote Sensing and an Artificial Neural Network. *Water Air Soil Pollut.* **2012**, *223*, 4875–4887. [[CrossRef](#)]

15. Ye, T.; Ziqi, G.; Yanchao, Q.; Xia, L.; Fei, X. Remote sensing of water quality monitoring in Guanting Reservoir. *Acta Ecol. Sin.* **2015**, *35*, 2217–2226. [[CrossRef](#)]
16. Bresciani, M.; Cazzaniga, I.; Austoni, M.; Sforzi, T.; Buzzi, F.; Morabito, G.; Giardino, C. Mapping phytoplankton blooms in deep subalpine lakes from Sentinel-2A and Landsat-8. *Hydrobiologia* **2018**, *824*, 197–214. [[CrossRef](#)]
17. Sagan, V.; Peterson, K.T.; Maimaitijiang, M.; Sidike, P.; Sloan, J.; Greeling, B.A.; Maalouf, S.; Adams, C. Monitoring inland water quality using remote sensing: Potential and limitations of spectral indices, bio-optical simulations, machine learning, and cloud computing. *Earth-Sci. Rev.* **2020**, *205*, 103187. [[CrossRef](#)]
18. Ruiz, R.; Tedeschi, L.; Marini, J.; Fox, D.G.; Pell, A.; Jarvis, G.; Russell, J. The Effect of a Ruminant Nitrogen (N) Deficiency in Dairy Cows: Evaluation of the Cornell Net Carbohydrate and Protein System Ruminant N Deficiency Adjustment. *J. Dairy Sci.* **2002**, *85*, 2986–2999. [[CrossRef](#)]
19. H, K. Review of soil nitrogen and its research methods. *Subtrop. Soil Water Conserv.* **2018**, *30*, 64–67.
20. Mathew, M.M.; Rao, N.S.; Mandla, V.R. Development of regression equation to study the Total Nitrogen, Total Phosphorus and Suspended Sediment using remote sensing data in Gujarat and Maharashtra coast of India. *J. Coast. Conserv.* **2017**, *21*, 917–927. [[CrossRef](#)]
21. Valderrama, J.C. The simultaneous analysis of total nitrogen and total phosphorus in natural waters. *Mar. Chem.* **1981**, *10*, 109–122. [[CrossRef](#)]
22. Pellissier, P.A.; Ollinger, S.V.; Lepine, L.C.; Palace, M.W.; McDowell, W.H. Remote sensing of foliar nitrogen in cultivated grasslands of human dominated landscapes. *Remote Sens. Environ.* **2015**, *167*, 88–97. [[CrossRef](#)]
23. Wu, S.; Xie, P.; Wang, S.; Zhou, Q. Changes in the patterns of inorganic nitrogen and TN/TP ratio and the associated mechanism of biological regulation in the shallow lakes of the middle and lower reaches of the Yangtze River. *Sci. China Ser. D Earth Sci.* **2006**, *49*, 126–134. [[CrossRef](#)]
24. Dewidar, K.; Khedr, A. Water quality assessment with simultaneous Landsat-5 TM at Manzala Lagoon, Egypt. *Hydrobiologia* **2001**, *457*, 49–58. [[CrossRef](#)]
25. Oki, K.; Yasuoka, Y. Mapping the potential annual total nitrogen load in the river basins of Japan with remotely sensed imagery. *Remote Sens. Environ.* **2008**, *112*, 3091–3098. [[CrossRef](#)]
26. Pan Bang, L.; Yi Wei, N.; Wang, X.; Qin Hui, P.; Cheng, W.J.; Li, Q.Y. Inversion of the Lake Total Nitrogen Concentration by Multiple Regression Kriging Model Based on Hyperspectral Data of HJ-1A. *Spectrosc. Spectr. Anal.* **2011**, *31*, 1884–1888.
27. Feng, A.; Wu, C.; Wang, X.; Wang Hong, L.; Ming, Z.Y.; Qian, Z.; Alikas, K. Spatial character analysis on nitrogen and phosphorus diffuse pollution in Haihe River Basin by remote sensing. *China Environ. Sci.* **2019**, *39*, 2999–3008.
28. Kutser, T.; Paavel, B.; Verpoorter, C.; Ligi, M.; Soomets, T.; Toming, K.; Casal, G. Remote Sensing of Black Lakes and Using 810 nm Reflectance Peak for Retrieving Water Quality Parameters of Optically Complex Waters. *Remote Sens.* **2016**, *8*, 497. [[CrossRef](#)]
29. Peng, Y.T.; Jia, Y.W.; Yuan, Z. Conversion study on multi-spectral information of remote sensing images GF-1 WFV, Landsat-8 OLI and Sentinel-2A MSI. *J. East China Norm. Univ. Nat. Sci.* **2017**, *6*, 136–146.
30. Tan, X. Water Quality Characteristics and Integrated Assessment Based on Multistep Correlation Analysis in the Danjiangkou Reservoir, China. *J. Environ. Inform.* **2015**, *25*, 60–70. [[CrossRef](#)]
31. Jerlov, N.G. Marine Optics. *Remote Sens. Environ.* **1977**, *6*, 151–153.
32. Kirk, J.T.O. Light and Photosynthesis in Aquatic Ecosystems. *Q. Rev. Biol.* **1987**, *62*, 110.
33. Hansen, C.; Burian, S.; Dennison, P.E.; Williams, G. Spatiotemporal Variability of Lake Water Quality in the Context of Remote Sensing Models. *Remote Sens.* **2017**, *9*, 409. [[CrossRef](#)]
34. Bej, A.K.; Mccarty, S.C.; Atlas, R.M. Detection of coliform bacteria and *Escherichia coli* by multiplex polymerase chain reaction: Comparison with defined substrate and plating methods for water quality monitoring. *Appl. Environ. Microbiol.* **1991**, *57*, 2429–2432. [[CrossRef](#)] [[PubMed](#)]
35. Wang, B. Correlation Analysis between Ammonia Nitrogen and Total Nitrogen in Wastewater. *Environ. Sci. Manag.* **2015**, *40*, 101–109.
36. Zhang, Q.; Cai, Z.; Yang Wen, J.; Rong, X.R.; Alikas, K. Discussion on the relationship between ammonia nitrogen and total nitrogen in surface water. *Zhejiang Agric. Sci.* **2016**, *57*, 276–277.

